

New aspects of the low-energy structure of ^{211}At

V. Karayonchev,^{1,2} A. Blazhev,¹ J. Jolie,¹ A. Dewald,¹ A. Esmaylzadeh ,¹ C. Fransen,¹ G. Häfner,¹ L. Knafla ,¹
C. Müller-Gatermann ,^{1,*} G. Rainovski,³ J.-M. Régis,¹ K. Schomacker,¹ and P. Van Isacker⁴

¹*Institut für Kernphysik, Universität zu Köln, 50937 Köln, Germany*

²*TRIUMF, 4004 Wesbrook Mall, Vancouver, British Columbia V6T 2A3, Canada*

³*Faculty of Physics, St. Kliment Ohridski University of Sofia, 1164 Sofia, Bulgaria*

⁴*Grand Accélérateur National d'Ions Lourds, CEA/DRF-CNRS/IN2P3, Bvd Henri Becquerel, F-14076 Caen, France*



(Received 16 May 2022; revised 29 August 2022; accepted 13 September 2022; published 20 October 2022)

Lifetimes of low-energy states in the semimagic nucleus ^{211}At were measured employing the recoil-distance Doppler shift and the Doppler-shift attenuation methods. The deduced transition probabilities are compared to two shell-model calculations, one using the modified Kuo-Herling interaction in a multi- j model space and the other using a semiempirical interaction for protons confined to the single- j $0h_{9/2}$ orbital. The Kuo-Herling calculations overestimates some of the ground-state transition probabilities, possibly due to contributions not included in the calculated ground-state wave function of ^{211}At . A strong underestimation of the $E2$ strengths involving the $7/2_1^-$ state is also observed. Therefore, a modification of a single two-body matrix element of the Kuo-Herling interaction is introduced which improves the agreement with the experimental data significantly. The calculations in the single- j approximation agree very well with the measured transition probabilities, indicating that seniority can be regarded as a good quantum number in ^{211}At .

DOI: [10.1103/PhysRevC.106.044321](https://doi.org/10.1103/PhysRevC.106.044321)

I. INTRODUCTION

The nuclear shell model arguably provides the most successful description of the atomic nucleus. In this model nucleons occupy shells that are formed by a central potential, a mean field, created by the nucleons themselves, with a strong spin-orbit term [1]. A two-body residual interaction between the nucleons introduces mixing of the different configurations. A starting point in constructing the residual nuclear interaction is usually a realistic effective nucleon-nucleon potential. Such are the approaches of Kuo and Herling [2] based on the Hamada-Johnson potential [3] and the $V_{\text{low-}k}$ approach [4,5] based on potentials such as Bonn [6], N3LO [7], and Argonne [8]. However, a renormalization is necessary for the energy regime of nucleons confined to a nucleus, which requires experimental input. The study of nuclei with only a few valence nucleons is the first step in understanding and tuning the nuclear residual interaction. With only a few nucleons, the number of the possible configurations is limited and permits calculations in a large basis without the need for truncations. The predictions of the shell model can then be compared to experimental observables to test the adequacy of the used residual interaction.

The ^{208}Pb nucleus is the heaviest doubly magic nucleus. Nuclei in its vicinity have attracted significant experimental and theoretical interest. Experimentally, nuclei around the

stable ^{208}Pb could be accessed relatively easy, and there is a large amount of spectroscopic data already available. Theoretically, the fact that ^{208}Pb has a good doubly magic character has motivated many shell-model calculations [9–14], which were successful at describing the energy spectrum of the nuclei in the vicinity of ^{208}Pb . Particularly successful has been the residual interaction of Kuo and Herling [2] and its modification proposed in Ref. [11]. However, experimental information on transition probabilities in nuclei in this region is limited. Only recently, transition probabilities were experimentally obtained for the lower-lying states of the Po isotopes [15–18]. Transition probabilities are important observables since they are often sensitive to small contributions in the nuclear wave functions, which have a small effect on the energy spectrum. Recent lifetimes measurements in ^{210}Po [19] and ^{212}Po [16] revealed that shell-model calculations with the modified Kuo-Herling interaction [11] significantly overestimate the $B(E2; 2_1^+ \rightarrow 0_1^+)$ value while accounting well for the observed energy spectrum and the other transition rates within the yrast band. A similar problem occurs also for the recently developed H208 interaction [14]. This discrepancy has been assumed to be due to the presence of higher-order particle-hole excitations in the ground state of ^{210}Po [20], which are not taken into account in the calculations. To investigate this assumption, our group has studied the neighboring ^{211}At nucleus populated in a fusion-evaporation reaction using the fast-timing technique [20]. Even though the deduced $B(E2; 17/2_1^- \rightarrow 13/2_1^-)$ value was slightly overestimated by the shell-model calculation, no firm conclusion was possible based solely

*Present address: Physics Division, Argonne National Laboratory, Argonne, Illinois 60439, USA

on this transition rate. In the same study, ^{211}At was discussed in the framework of a shell-model calculation with a semiempirical interaction, assuming that the protons are confined to the $0h_{9/2}$ orbital. The single- j calculation gave a good description of the low-energy levels of ^{211}At and also reproduced the measured $B(E2; 17/2_1^- \rightarrow 13/2_1^-)$ value accurately. However, the situation for the low-spin states remained unclear.

To further investigate the effect of particle-hole excitations on the low-energy structure of ^{211}At and to test the single- j calculation, recoil-distance Doppler-shift (RDDS) and Doppler-shift attenuation (DSA) lifetime measurements were performed. Specifically, this paper reports on the measurement of the lifetimes of the $7/2_1^-$, $7/2_2^-$, $5/2_1^-$, $13/2_1^-$, $11/2_1^-$, and $13/2_1^+$ states in ^{211}At .

II. EXPERIMENT

The ^{211}At nucleus was populated in the $^{209}\text{Bi}(^{16}\text{O}, ^{14}\text{C})^{211}\text{At}$ reaction. A ^{16}O beam with energy of 84 MeV was provided by the FN-Tandem accelerator at the University of Cologne. The target used for the RDDS experiment was a 1.1 mg/cm^2 ^{209}Bi evaporated on a 0.4 mg/cm^2 Mg backing facing the beam. It was stretched inside the Cologne Plunger device [21] in parallel to a 1.1 mg/cm^2 Mg stopper used to stop the ejecting ^{211}At nuclei. The target used in the DSA measurement was a 0.5 mg/cm^2 ^{209}Bi evaporated on a 1.5 mg/cm^2 Mg backing. γ rays emitted from the targets were detected by eleven high-purity germanium detectors positioned in two rings at 45° and 142° . Recoiling beam-like nuclei were detected by an array of six solar cells placed at backward angles, covering angles between 120° and 165° . The data was recorded in triggerless mode and sorted offline. The RDDS data was taken at six target-to-stopper distances (5, 15, 30, 50, 100, 300 μm) determined relative to a zero point of 27(2) which has been obtained by the capacitive method [21,22]. These distances were kept constant by the active feed-back system of the Cologne Plunger device [21]. Additionally, data was collected without the active feed-back system, at electrical contact between the target and the stopper, achieving smaller distances than 27 μm . This measurement run served as a feasibility test for the later conducted DSA measurement. The particle spectrum observed in the solar cells is displayed in Fig. 1. A clear distinction could be made between the four main channels—the Coulomb excitation of the target, the single-proton, the two-proton, and the α -transfer reactions. A gate set on the group of particles as indicated in Fig. 1 yields a clean γ -ray spectrum of ^{211}At displayed in Fig. 2. The information on the observed γ rays is summarized in Table I. A previously known transition feeding the $17/2_1^-$ state from a state of unknown spin and parity [23] is observed in the experiment and is designated as “A”. The intensity of this transition could not be determined reliably, since it lays on the neutron edge, produced by the $(n, n'\gamma)$ reaction on the ^{74}Ge of the germanium detectors. The intensity of the $23/2_1^- \rightarrow 21/2_1^-$ transition could not be determined either, because the transition energy coincides with the

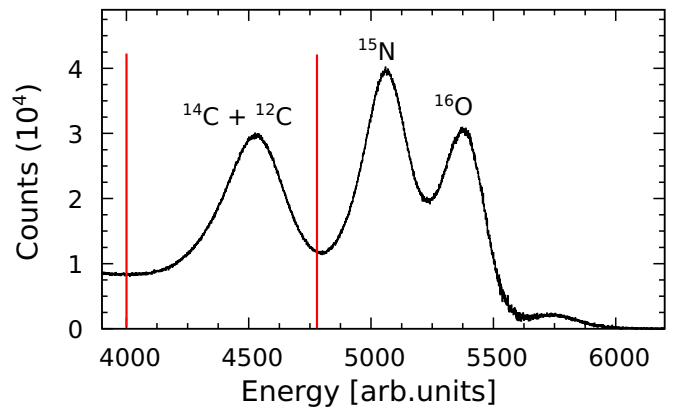


FIG. 1. Spectrum of back-scattered particles in coincidence with one γ ray obtained during the RDDS experiment. The main reaction products are indicated. The vertical red lines indicate the gate used to obtain the γ -ray spectra used in the experiment.

511-keV annihilation peak commonly present in in-beam γ -ray experiments. Using γ - γ coincidences a level scheme relevant for this experiment was built and is displayed in Fig. 3.

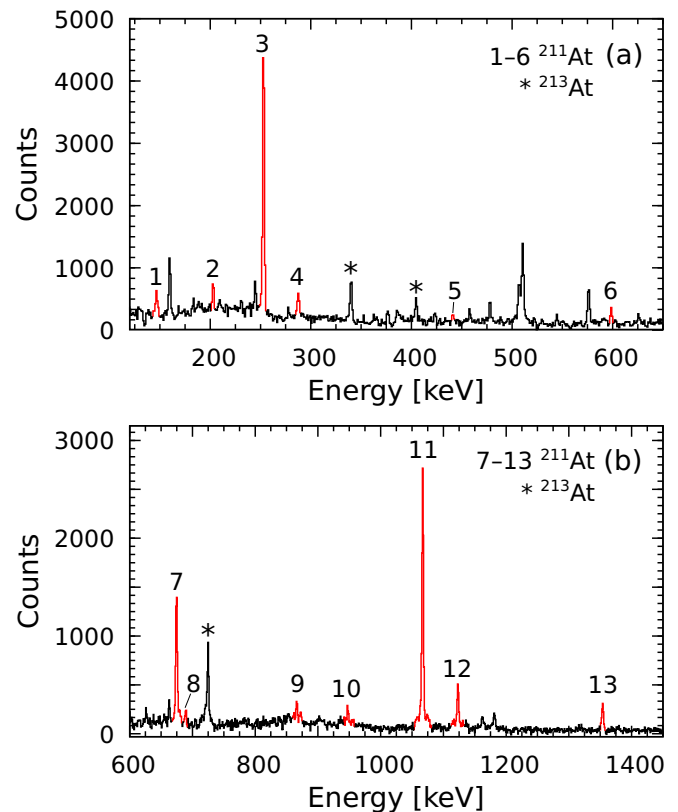


FIG. 2. Single γ rays of both detector rings in coincidences with the ^{14}C particles, as indicated in Fig. 1, taken at electrical contact. The transitions belonging to ^{211}At are indicated and colored in red. A list of the transitions is given in Table I.

TABLE I. γ -ray transitions observed in the $^{209}\text{Bi}(^{16}\text{O}, ^{14}\text{C})^{211}\text{At}$ reaction. Transition intensities are normalized to the $13/2_1^- \rightarrow 9/2_1^-$ transition intensity.

Index	Transition	Energy [keV]	Intensity [%]
1	$15/2_1^- \rightarrow 11/2_1^-$	147	2.6(10)
2	$15/2_1^- \rightarrow 13/2_1^-$	203	4.0(10)
3	$17/2_1^- \rightarrow 13/2_1^-$	254	44.5(20)
4	$13/2_1^+ \rightarrow 13/2_1^-$	288	5.0(10)
5	$3/2_1^- \rightarrow 7/2_1^-$	442	2.3(10)
6	$A \rightarrow 17/2_1^-$	599	—
7	$7/2_1^- \rightarrow 9/2_1^-$	674	37.0(20)
8	$25/2_1^+ \rightarrow 23/2_1^-$	689	2.0(10)
9	$7/2_2^- \rightarrow 9/2_1^-$	866	12.0(20)
10	$5/2_1^- \rightarrow 9/2_1^-$	947	10.0(15)
11	$13/2_1^- \rightarrow 9/2_1^-$	1067	100.0(6)
12	$11/2_1^- \rightarrow 9/2_1^-$	1123	27.0(20)
13	$13/2_1^+ \rightarrow 9/2_1^-$	1355	10.5(7)
—	$23/2_1^- \rightarrow 21/2_1^-$	511	—

III. ANALYSIS AND RESULTS

A. RDDS analysis

The RDDS technique in combination with Bateman equations was used to extract the lifetimes longer than 5 ps. For a detailed review of the technique, the reader is referred to the review article. [21].

The average speed of $v = 1.09(9)\% c$ of the ejected ^{211}At nuclei was determined directly by measuring the Doppler shift of the strongest peaks observed in the experiment. This speed was used to determine the average time of flight t between the target and the stopper for each distance, which was used in Bateman equations. Due to the relatively large target thickness, the stopping of the ^{211}At ions inside the target has an effect on the velocity distribution, which might lead to a deviation in the determined t . To check if there is a considerable effect due to the velocity distribution, we have performed a

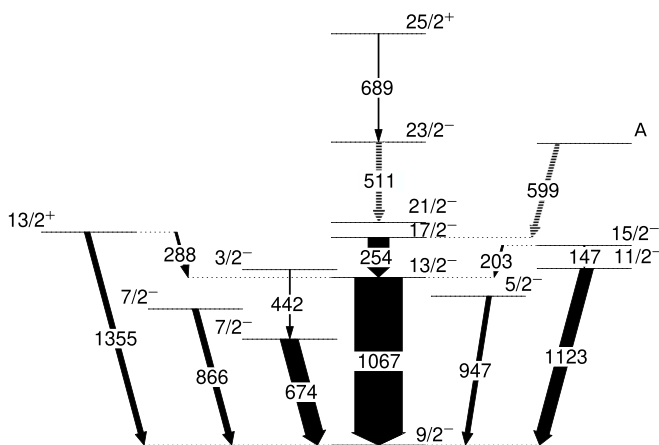


FIG. 3. Level scheme of ^{211}At populated in the $^{209}\text{Bi}(^{16}\text{O}, ^{14}\text{C})^{211}\text{At}$ two-proton transfer reaction at 84 MeV beam energy. The line thicknesses are proportional to the γ -ray transition intensities given in Table I.

Monte Carlo simulation in the framework of GEANT4 [27] and the APCAD software [26]. In the simulation, the RDDS target and the stopper were placed some certain distance away. ^{16}O beam was allowed to impinge on the target and as a result ^{211}At are created in the bismuth layer of the target in a transfer reaction. The ^{211}At ions then undergo stopping inside the target, a drift in the vacuum between the target and the stopper, and, finally, a rapid stopping inside the magnesium stopper. We have used this simulation to determine the average time it takes the ^{211}At ions to stop inside the stopper after they are created inside the target. This time is in good agreement with the average time calculated using the velocity of $v = 1.09(9)\% c$.

When determining the lifetime of a given state using the Bateman equations only the lifetime of the state was used as a fit variable. All other parameters, i.e., the lifetime of the states feeding the state of interest and the feeding intensities were fixed. Accordingly, the lifetimes of the higher-lying states were determined first and were used as fixed parameters when determining the lifetimes of the lower-lying states. Some of the previously observed low-intensity branchings [23] from states populated in this experiment were not observed explicitly in this experiment but they were taken into account when conducting the lifetime measurements. To obtain the $R(t)$ ratios of a given transition, the shifted and the unshifted components were fitted for each distance using two Gaussian function. The width of the Gaussian functions and their positions were kept constant during the fit for each of the distances.

The fit to the data of the $7/2_1^- \rightarrow 9/2_1^-$ transition for three of the distances of the forward detector ring is shown in Figs. 4(a)–4(c). Unfortunately, the $9_1^+ \rightarrow 7_1^+$ transition in ^{210}At , which is populated in the $(^{16}\text{O}, ^{15}\text{C})$ reaction has an energy of 675.5 keV, very similar to the energy of the $7/2_1^- \rightarrow 9/2_1^-$ transition in ^{211}At and both peaks appears as a doublet. To obtain the correct intensity of the $7/2_1^- \rightarrow 9/2_1^-$ transition, γ - γ coincidences were sorted. A gate was placed on both the shifted and the unshifted components of the $7_1^+ \rightarrow 5_1^+$ transition in ^{210}At which is in coincidences with the $9_1^+ \rightarrow 7_1^+$ transition. The peak of the $9_1^+ \rightarrow 7_1^+$ transitions appeared to be completely stopped and to have no time evolution. Its coincidences intensity has been measured. By measuring the intensity of the $7_1^+ \rightarrow 5_1^+$ transition in the singles spectrum and correcting for the efficiency of the detectors, the singles intensity of the $9_1^+ \rightarrow 7_1^+$ transition in ^{210}At has been determined as 9(2)% of the $7/2_1^- \rightarrow 9/2_1^-$ transition intensity in ^{211}At . This can be done because the 7_1^+ decays primarily by the $7_1^+ \rightarrow 5_1^+$ transition [23]. A correction has been applied to the unshifted component of the $7/2_1^- \rightarrow 9/2_1^-$ transition. The corrected data points of the $R(t)$ ratios for all the distances are fitted using the Bateman equations. To obtain the value of the lifetime a Monte Carlo simulation was performed. All the input parameters used in the fit are independently varied within the corresponding experimental uncertainties before performing the fit. The uncertainties of the $R(t)$ values are increased by a factor of two to accommodate for possible systematic errors arising when choosing the background parametrization used

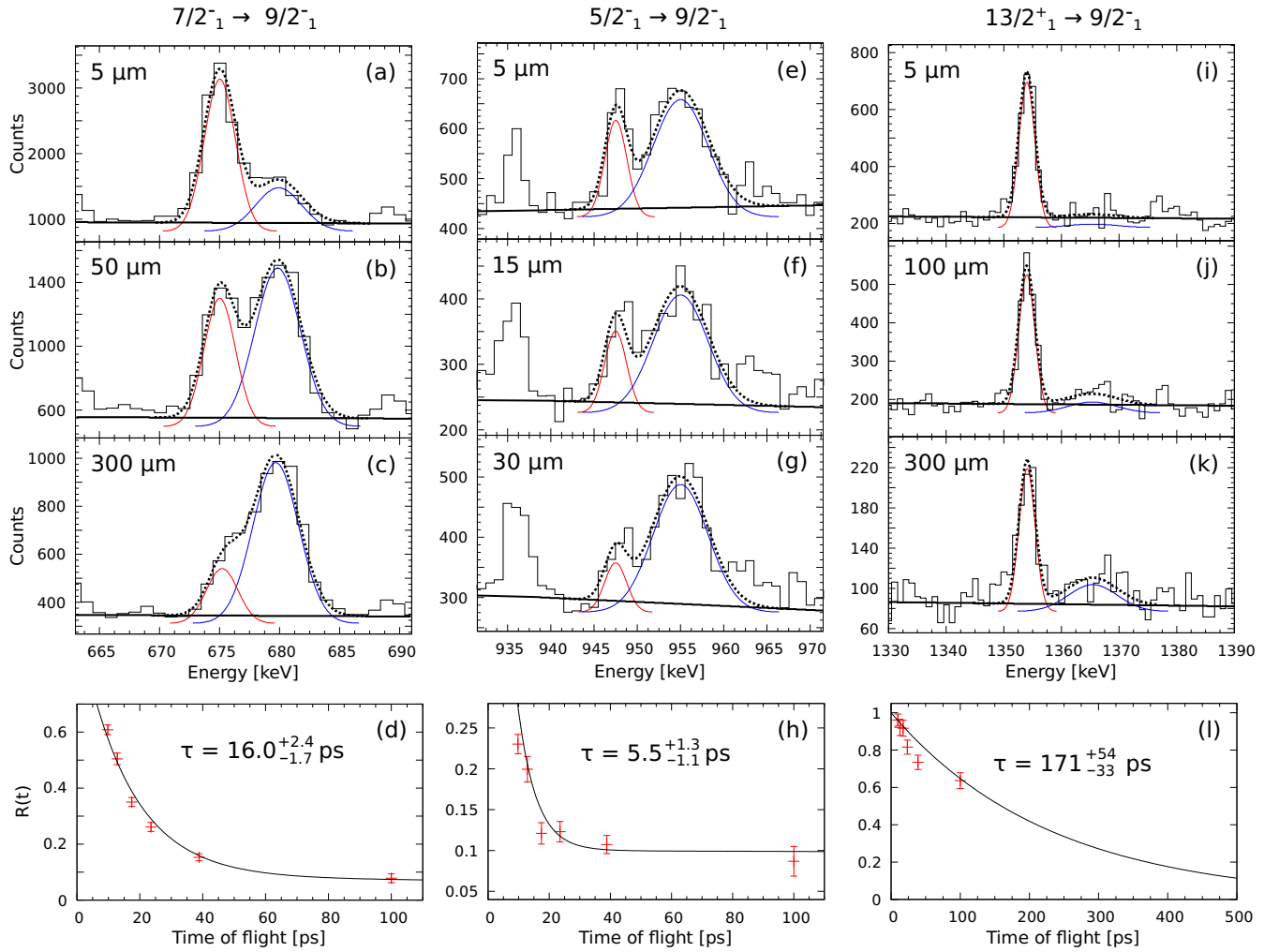


FIG. 4. (a),(b),(c) Fits to the $7/2_1^- \rightarrow 9/2_1^-$ transition (dotted black line) of the forward-detector ring for three distances used to determine the intensity of the shifted (blue solid line) and the unshifted components (red solid line). The black solid line is the background parametrization. (d) The Bateman fit to the obtained $R(t)$ of the $7/2_1^- \rightarrow 9/2_1^-$ transition for all distance used to obtain the lifetime of the $7/2_1^-$ state, together with the obtained lifetime. (e),(f),(g),(h) are the same as (a),(b),(c),(d) but for the $5/2_1^-$ state. (i),(j),(k),(l) are same as (a),(b),(c),(d) but for the $13/2_1^+$ state.

when determining the intensities of the shifted and unshifted components from the experimental spectrum. This process is repeated 10^6 times and the results from the fits are written in a histogram. The distribution is almost symmetric, with a small sloping towards the higher lifetimes. The value of the lifetime is defined as the mean of this distribution and the upper and the lower limits as the σ_+ and σ_- intervals around the mean value. The feeding coming from the $7/2_2^-$ and the $3/2_1^-$ states was taken into account when determining the lifetime of the $7/2_1^-$ state. The intensity of the $3/2_1^- \rightarrow 7/2_1^-$ transition is measured in this experiment and its lifetime is taken from the Ref. [23]. The intensity of the $7/2_2^- \rightarrow 7/2_1^-$ transition is determined based on the intensity of the $7/2_2^- \rightarrow 9/2_1^-$ transition and the known branching ratio taken from Ref. [23] and its lifetime is determined in this experiment (see next section). The resulting fit for the forward detector ring and the data points are displayed in Fig. 4(d). The resulting lifetime is $16_{-1.7}^{+2.4}$ ps. An analogous procedure

performed for the backward detector ring yields a lifetime of $14.8_{-1.6}^{+2.3}$ ps.

Similarly, the lifetime of the $5/2_1^-$ state was determined using the $5/2_1^- \rightarrow 9/2_1^-$ transition. An analysis was only possible for the forward detector ring due to the presence of an unidentified transition with 936 keV energy. The fits to the spectra used to obtain the decay curve are displayed in Figs. 4(e)–4(g), where the 936-keV peak is also seen. The corresponding $R(t)$ ratios are fitted and the result is displayed in Fig. 4(h). The resulting lifetime is $5.5_{-1.1}^{+1.3}$ ps. The lifetime of the $13/2_1^+$ has been determined in a similar way. The fit to obtain the $R(t)$ ratios of the forward detector ring is displayed in Figs. 4(i)–4(k). The Bateman fit to the data points is displayed in Fig. 4(l) and yields a lifetime of 171_{-33}^{+54} ps. The procedure for the backward detector ring gives a lifetime of 313_{-64}^{+137} ps. The results of the lifetime analysis using the RDDS technique are summarized in Table II. The adopted values given in the table are obtained by convoluting the

TABLE II. Measured and adopted lifetimes of excited states in ^{211}At using the RDDS and DSAM methods.

State	Lifetime [ps]		Adopted
	Forward	Backward	
	RDDS		
$7/2_1^-$	$16_{-1.7}^{+2.4}$	$14.8_{-1.6}^{+2.3}$	15.4(14)
$5/2_1^-$	$5.5_{-1.1}^{+1.3}$	—	5.5$_{-1.1}^{+1.3}$
$13/2_1^+$	171_{-33}^{+54}	313_{-64}^{+137}	242$_{-37}^{+68}$
	DSAM		
$7/2_2^-$	3.0(4)	3.3(4)	3.15(30)
$13/2_1^-$	2.7(3)	2.8(3)	2.75(21)
$11/2_1^-$	3.3(3)	3.1(3)	3.2(2)

distributions for the forward and backward detector rings obtained using the Monte Carlo procedure.

B. DSA analysis

The shorter lifetimes (<5 ps) were determined using the DSA method. Here, only the basic principles of the DSA method are presented. For a detailed review of the method, the reader is referred to Refs. [24,25].

Excited nuclei produced in the target are allowed to recoil in a stopping material. While slowing down, the nuclei emit γ rays in-flight which appear Doppler shifted in the spectrum of the germanium detectors. Since the slowing down of the nuclei inside the stopper is a continuous process, the γ -ray peak observed in the detectors display a Doppler-broadened lineshape. If the slowing down process of the nuclei is known, the mean lifetime of the excited state emitting the γ rays could be extracted from a fit to the Doppler-broadened lineshape. The DSA analysis was performed using the program APCAD [26]. In APCAD, the stopping of the ^{16}O beam in the target and the stopping of the recoiling ^{211}At ions in the target and the backing are modeled using a Monte Carlo simulation in the framework of GEANT4 [27]. The electronic and nuclear stopping powers are taken from SRIM [28]. The nuclear stopping powers were reduced by 30% to account for microchanneling effects [29]. If the nuclear stopping reduction factor between is varied between 20% to 40% the results for the deduced lifetimes are altered by less than 4%. The doubly differential cross section of the $^{209}\text{Bi}(^{16}\text{O}, ^{14}\text{C})^{211}\text{At}$ reaction, which defines the geometry of the reaction, has been calculated using the GRAZING code [30,31]. After the individual traces of the ^{211}At ions are simulated, APCAD projects the spectra on the detectors, taking into account the detector geometry and intrinsic response and the kinematic restrictions imposed by the solar cells. The intrinsic detector response is a Gaussian with a small low-energy tailing. The resulting Doppler-broadened lineshapes are then fitted to the experimental spectra using only the lifetime as a fit parameter. The feeding of the state of interest from other states has also been taken into account. The uncertainties of the lifetimes determined in the following analysis account for the statistical error during the fit and the systematic errors that arises when assuming 10%

TABLE III. Measured and calculated $B(E2)$ values for transitions in ^{210}Po and ^{211}At . The table is taken from Ref. [20] and expanded with the new data.

$J_i^\pi \rightarrow J_f^\pi$	$B(E2; J_i^\pi \rightarrow J_f^\pi) [e^2\text{fm}^4]$			
	Expt ^a	Eq. (1)	KHP	KHP*
$2_1^+ \rightarrow 0_1^+$	136(21) ^b	136(21)	260	237
$4_1^+ \rightarrow 2_1^+$	331(13)	331(13)	331	336
$6_1^+ \rightarrow 4_1^+$	227(5) ^c	227(5)	227	226
$8_1^+ \rightarrow 6_1^+$	83(3)	83(3)	90	91
$3/2_1^- \rightarrow 5/2_1^-$	955(104)	678(9)	740	756
$3/2_1^- \rightarrow 7/2_1^-$	30(3)	—	0.7	24.5
$3/2_1^- \rightarrow 7/2_2^-$	133(13)	94(4)	130	115
$5/2_1^- \rightarrow 7/2_2^-$	—	83(10)	107	81.0
$5/2_1^- \rightarrow 9/2_1^-$	$195_{-37}^{+49\text{d}}$	195(12)	279	259
$7/2_1^- \rightarrow 9/2_1^-$	$108_{-16}^{+18\text{d}}$	—	14.7	128
$7/2_2^- \rightarrow 9/2_1^-$	$400_{-36}^{+43\text{d}}$	419(13)	459	314
$11/2_1^- \rightarrow 7/2_2^-$	—	95(6)	102	96.4
$11/2_1^- \rightarrow 9/2_1^-$	$141_{-8}^{+9\text{d}, \text{e}}$	149(7)	154	140
$11/2_1^- \rightarrow 13/2_1^-$	—	266(6)	252	248
$13/2_1^- \rightarrow 9/2_1^-$	$213_{-15}^{+18\text{d}}$	226(11)	291	273
$15/2_1^- \rightarrow 11/2_1^-$	127(22)	167(4)	169	169
$15/2_1^- \rightarrow 13/2_1^-$	28(6)	48(2)	50	50
$17/2_1^- \rightarrow 13/2_1^-$	300(20) ^f	306(6)	332	334
$17/2_1^- \rightarrow 15/2_1^-$	—	86(4)	82	81.7
$21/2_1^- \rightarrow 17/2_1^-$	198(7)	173(3)	191	190

^aFrom Refs. [23,36] unless otherwise indicated.

^bFrom Ref. [19].

^cFrom Ref. [37].

^dThis work.

^eAssuming a pure $E2$ transition.

^fFrom Ref. [20].

uncertainty in the stopping powers and 10% uncertainty in the target thickness. Additionally, the influence of the background parametrization was investigated and was included in the error. In the error determination of the lifetimes, additional slow feeding with intensities up to the observation was also assumed. For the energy region of interest this amounts to 1% of the $13/2_1^- \rightarrow 9/2_1^-$ transition intensity. The uncertainty of the lifetimes has been symmetrized by taking the larger of either the low or high uncertainty limits. The lifetime of the $7/2_2^-$ has been determined by performing a DSA fit to the lineshape of the $7/2_2^- \rightarrow 9/2_1^-$ transition. The fits for the forward and the backward detector rings are displayed in Figs. 5(a) and 5(b). The resulting lifetimes are 3.0(4) ps and 3.3(4) ps, respectively. Similarly, the lifetimes of the $13/2_1^-$ and $11/2_1^-$ states have been determined by DSA fits to the lineshapes of the $13/2_1^- \rightarrow 9/2_1^-$ and the $11/2_1^- \rightarrow 9/2_1^-$ transitions, respectively. The results of the fits are displayed in Figs. 5(c)–5(f).

The results of the performed lifetime analysis are summarized in Table II. With the newly measured lifetimes and the branching ratios, conversion coefficients, and the multipolarity mixing ratios from Ref. [23], reduced transition probabilities were calculated and are listed in Table III. Due to the large uncertainty of the multipolarity-mixing ratio $\delta(E2/M1) = -0.06(18)$ of the $7/2_2^- \rightarrow 7/2_1^-$ transition [32],

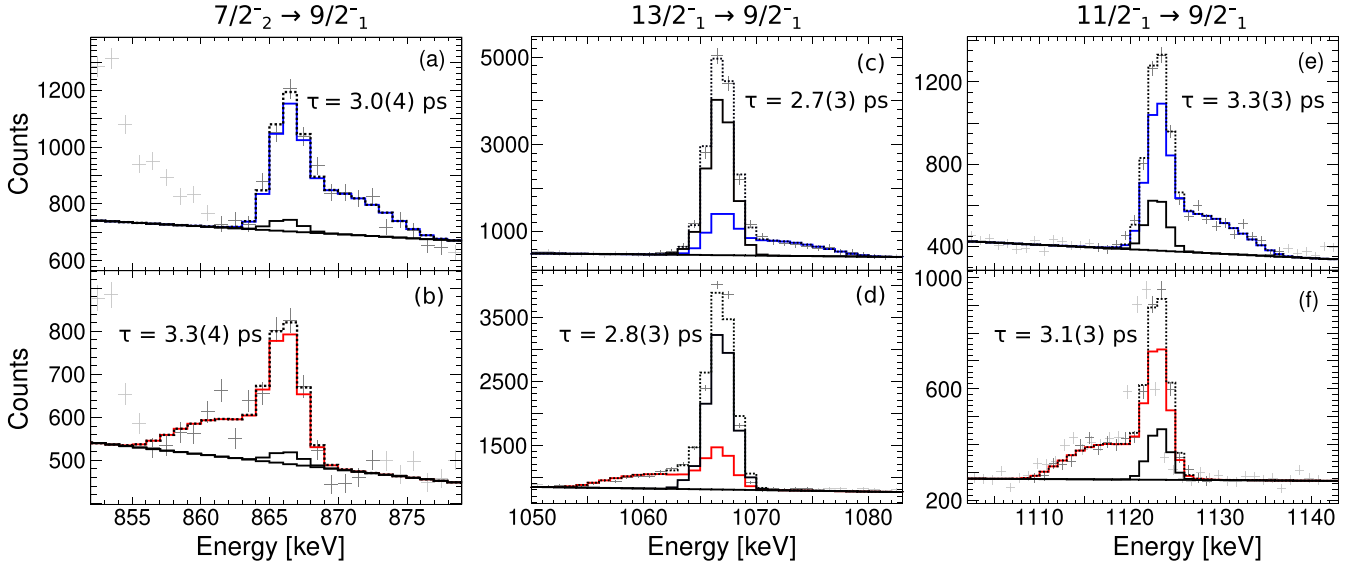


FIG. 5. (a) DSA fit to the Doppler-broadened lineshape of the $7/2_2^- \rightarrow 9/2_1^-$ transition of the forward detector ring used to determine the lifetimes of the $7/2_2^-$ state. The black solid line is the background parametrization, the solid black peak represents the long-lived feeding of the $7/2_2^-$ state, the blue solid line is the DSA fit to the spectrum excluding the long-lived feeding and the dotted black line is the DSA fit to the data including the long-lived feeding. (b) Same as (a) but for the backward detector ring and the DSA fit excluding the long-lived feeding is a solid red line. (c),(d) same as (a),(b) but for the $13/2_1^-$ state. (e),(f) same as (a),(b) but for the $11/2_1^-$ state.

the reduced transition probability $B(E2, 7/2_2^- \rightarrow 7/2_1^-)$ could not be determined with sufficient accuracy. To obtain a proper value of the $B(E2, 7/2_2^- \rightarrow 7/2_1^-)$ a more accurate measurement of the multipolarity-mixing ratio is needed. Nonetheless, within the error bars the transition shows a dominant $M1$ character. In addition, there is also a discrepancy in the intensity of the $7/2_2^- \rightarrow 7/2_1^-$ transition. In the fusion-evaporation reactions $^{208}\text{Pb}(^7\text{Li}, 3n)$ [33] and $^{209}\text{Bi}(\alpha, 2n)$ [34] the branching of this transition has been reported as 4.4(13) and 7.7, respectively, while in the electron capture of ^{211}Rn [35] it has been determined as 11.4(6). The value of 11.4(6) has been adopted in the Nuclear Data Sheets. [23]. This value leads to a large $B(M1, 7/2_2^- \rightarrow 7/2_1^-) = 0.213_{-0.023}^{+0.027} \mu_N^2$ value. However, the branching of the $7/2_2^- \rightarrow 7/2_1^-$ transition needs to be experimentally fixed in order to get unambiguous transition probabilities.

IV. DISCUSSION

The newly extracted $B(E2)$ values are compared to two shell-model calculations, a calculation using a semiempirical interaction for three protons in a single $j = 9/2$ orbital and a large-scale shell-model calculation using the modified Kuo-Herling interaction in a multi- j model space. The calculations are already partly reported and discussed in Ref. [20]. In the following subsections, we concentrate mainly on the newly acquired reduced transition probabilities. In addition we also introduce a modification to a single two-body matrix element of the Kuo-Herling interaction which significantly improves the agreement with the experimental data both for ^{211}At and the neighboring ^{210}Po . At the end of the section, the $13/2_1^+ \rightarrow 9/2_1^-$ transition is discussed in the framework of the theory of finite Fermi systems with an effective $M2$ operator.

A. Single- j calculation

Since the ^{211}At nucleus has only three valence protons above the doubly closed shell nucleus ^{208}Pb , it is clear that its low-energy structure will be dominated by the couplings of the three protons in the $0h_{9/2}$ orbital. It is, therefore, reasonable to assume that the structure of ^{211}At can be described in a single- j approximation, limiting the model space only to the three protons in the $0h_{9/2}$ orbital. A shell-model description confined to a single- j orbital has the advantage that simple analytic predictions can be made for the physical properties of the nuclei [38]. If seniority is conserved and the residual interaction is of two-body character, the energy spectrum of the three-nucleon system (^{211}At) can be related to that of the two-nucleon system (^{210}Po). This was done for ^{211}At in Ref. [20] and showed a good agreement with the observed energy spectrum. Similarly, electric quadrupole matrix elements in the three-particle system can be related to those of the two-particle system as

$$B(E2; j^3 J_i \rightarrow j^3 J_f) = \left(\sum_R g_j(J_i, J_f, R) \sqrt{B_R} \right)^2 \quad (1)$$

with $B_R = B(E2; j^2 R \rightarrow j^2 R - 2)$, where the $B(E2)$ values on the left-hand side refer to the three-particle nucleus and those on the right-hand side to the two-particle nucleus. The relation (1) is derived in Ref. [20], where also the expressions for the coefficients $g_j(J_i, J_f, R)$ are given. One assumption required for the relation to hold is the conservation of seniority. If in addition the $E2$ operator is of one-body character with a single effective charge, then Eq. (1) is satisfied. However, the relation has wider applicability and still holds for a one-body $E2$ operator with state-dependent effective charges. A one-body $E2$ operator with state-dependent effective charges is similar but not equivalent to a one-plus-two-body $E2$

TABLE IV. Experimental and calculated excitation energies (in MeV) of levels in ^{210}Po and ^{211}At . The table is taken from Ref. [20] and expanded with the KHP* calculations. Experimental data is taken from Refs. [23,36].

Nucleus		0_1^+	2_1^+	4_1^+	6_1^+	8_1^+						
^{210}Po	Expt	0.000	1.181	1.427	1.473	1.557						
	KHP	0.000	1.200	1.466	1.482	1.533						
	KHP*	0.000	1.179	1.466	1.482	1.533						
^{211}At		$9/2_1^-$	$7/2_1^-$	$7/2_2^-$	$5/2_1^-$	$13/2_1^-$	$3/2_1^-$	$11/2_1^-$	$15/2_1^-$	$17/2_1^-$	$21/2_1^-$	$23/2_1^-$
	Expt	0.000	0.674	0.866	0.947	1.067	1.116	1.123	1.270	1.320	1.416	1.927
	KHP	0.000	0.733	0.928	1.073	1.123	1.282	1.216	1.357	1.391	1.441	1.863
	KHP*	0.000	0.706	0.929	1.052	1.122	1.288	1.217	1.364	1.398	1.448	1.869

operator with constant effective charges. While both operators can be made to exactly reproduce the $B(E2)$ values of the two-nucleon system, the predicted $E2$ transition rates will diverge for higher nucleon numbers.

With use of Eq. (1) the reduced transition probabilities in ^{211}At have been calculated based on those in ^{210}Po , taking into account the experimental uncertainties. The results are presented in Table III. The $7/2_1^-$ and $13/2_1^+$ levels, of which lifetimes have been measured in this experiment, are outside the model space of the single- j approximation. The newly measured $B(E2)$ values agree with the calculated values within the experimental uncertainties. The good agreement of this simple model with the experiment indicates that the assumptions made in the model are to some extent true, i.e., the residual nuclear interaction conserves seniority and the $E2$ operator can be assumed of one-body character with state-dependent effective charges.

A microscopic justification of the single- j assumption can be based on the fact that the Fermi levels for protons that occupy $0h_{9/2}$ and for neutrons that occupy $2p_{1/2}$ are separated by 3.6 MeV [11,39]. The large energy difference of the Fermi levels leads to small neutron-proton couplings, resulting in relatively pure proton excitations. Additionally, the two orbitals have a large spin difference, further weakening the neutron-proton interaction.

An advantage of the single- j description is that correlations in the wave functions that play a role in the transition probabilities in the two-particle system are inherently carried over to the three-particle system. As a result, the predictions of the single- j calculation agree better with the measured reduced transition probabilities than the shell-model calculation with the KHP residual interaction.

While in this single- j study higher-order effects are considered in the $E2$ operator, the residual interaction is assumed to be of two-body character. It would be of interest to include effects of a three-body interaction. However, for the complete determination of the three-body components the experimental excitation energy of the second $9/2^-$ level in ^{211}At is needed, which has not been reported up to now. A three-body interaction might be important for ^{213}Fr where one might expect the breaking of seniority selection rules as it is located five valence protons away from the ^{208}Pb core.

B. Multi- j shell-model calculation

The large-scale shell-model calculation is performed using the modified Kuo-Herling particle (KHP) interaction [11] in a multi- j model space, which includes the proton orbitals $0h_{9/2}$, $1f_{7/2}$, $0i_{13/2}$, $1f_{5/2}$, $2p_{3/2}$, and $2p_{1/2}$ above the ^{208}Pb core. The single-particle energies are taken from Ref. [11]. The calculations are performed with the code NUSHELLX@MSU [40] without any truncation. The results for the transition probabilities and the energy levels for both ^{210}Pb and ^{211}At are denoted with ‘KHP’ in the text and are presented in Tables III and IV, respectively. The newly measured $B(E2; 7/2_2^- \rightarrow 9/2_1^-)$ and $B(E2; 11/2_1^- \rightarrow 9/2_1^-)$ values are described well by the KHP calculation even though they are slightly overestimated. However, the experimental $B(E2; 5/2_1^- \rightarrow 9/2_1^-)$ and $B(E2; 13/2_1^- \rightarrow 9/2_1^-)$ values are significantly lower than the KHP predictions. As stated in Ref. [20], a possible explanation could be the presence of particle-hole excitations of second and higher orders, which are not included in the KHP effective interaction and are not part of the model space. Similarly, the presence of particle-hole excitations of higher-order in the ground state of ^{210}Po was also given as a plausible reason to explain the reduced collectivity of the $2_1^+ \rightarrow 0_1^+$ transition, which is overestimated by about a factor two in the KHP calculation. Indeed, the ground state of ^{211}At could be presented as a single proton coupled to the ground state of ^{210}Po . It appears that the discrepancy between the calculated and measured transition probabilities decreases when moving away from the ^{208}Pb core. It would be of great interest to continue this study in the heavier $N = 126$ isotones.

However, the KHP calculation underestimates the $B(E2; 7/2_1^- \rightarrow 9/2_1^-)$ and $B(E2; 3/2_1^- \rightarrow 7/2_1^-)$ experimental values by more than an order of magnitude. In an attempt to understand the origin of this discrepancy, various two-body matrix elements (TBME) of the KHP interaction were varied, and the influence on the nuclear structure of ^{210}Po and ^{211}At was investigated. The calculations were performed using the KSHELL program [41]. We have noticed that the $\langle 0h_{9/2}, 0h_{9/2} | \hat{V} | 0h_{9/2}, 1f_{7/2} \rangle_{J=2}$ TBME has a big influence on the $B(E2; 7/2_1^- \rightarrow 9/2_1^-)$ and $B(E2; 3/2_1^- \rightarrow 7/2_1^-)$ values. The variations in this TBME also influence the $B(M1; 7/2_2^- \rightarrow 7/2_1^-)$ value considerably and have a small but significant influence on

the $B(E2; 7/2_2^- \rightarrow 9/2_1^-)$ value as well as on the excitation energy of the first excited 2_1^+ state in the neighboring ^{210}Po . The dependence of all these observables in comparison with the experimental values is displayed in Fig. 6. The default value of the $\langle 0h_{9/2}, 0h_{9/2} | \hat{V} | 0h_{9/2}, 1f_{7/2} \rangle_{J=2}$ TBME is -0.02349 MeV and is the rightmost point in the figure. The agreement for this value is good only for the $B(E2; 7/2_2^- \rightarrow 9/2_1^-)$ value. However, by increasing the absolute value of the TBME, all the other four observables could be brought to a much better agreement with the experimental data while keeping the agreement for the $B(E2; 7/2_2^- \rightarrow 9/2_1^-)$ value reasonable, considering the fact it has a relatively large experimental uncertainty. A calculation with $\langle 0h_{9/2}, 0h_{9/2} | \hat{V} | 0h_{9/2}, 1f_{7/2} \rangle_{J=2} = -0.20$ MeV was performed and the results for the transition probabilities and the energy levels are labeled as KHP* and are displayed in Tables III and IV, respectively. This value was determined by χ^2 minimization procedure using the $B(E2; 7/2_1^- \rightarrow 9/2_1^-)$, $B(E2; 7/2_2^- \rightarrow 9/2_1^-)$, $B(M1; 7/2_2^- \rightarrow 7/2_1^-)$, and $B(E2; 3/2_1^- \rightarrow 7/2_1^-)$ transition rates. The overall agreement for both ^{211}At and ^{210}Po is considerably better than when using the default value of this TBME, most notably, the $B(E2; 7/2_1^- \rightarrow 9/2_1^-)$ and $B(E2; 3/2_1^- \rightarrow 7/2_1^-)$ values both agree with the experimental data. However, this calculation underestimates the $B(E2; 3/2_1^- \rightarrow 7/2_2^-)$ and $B(E2; 7/2_2^- \rightarrow 9/2_1^-)$ values, while the calculation with the default value of the TBME accounts for both transitions. Given the fact that the transitions involving the $7/2_1^-$ and $7/2_2^-$ states are most significantly influenced by the change in the value of the $\langle 0h_{9/2}, 0h_{9/2} | \hat{V} | 0h_{9/2}, 1f_{7/2} \rangle_{J=2}$ TBME it is logical to assume that the wave functions of these states will be most influenced by this change. In Fig. 7 the evolution of the occupation number of the leading configurations as a function of the $\langle 0h_{9/2}, 0h_{9/2} | \hat{V} | 0h_{9/2}, 1f_{7/2} \rangle_{J=2}$ TBME is displayed. The main configurations that play a role in those two wave functions are $(0h_{9/2})^2 1f_{7/2}$ and $(0h_{9/2})^3$. At the default value, the wave function of the $7/2_1^-$ is dominated by the $(0h_{9/2})^2 1f_{7/2}$ configuration, consistent with a single proton being excited from the $0h_{9/2}$ orbital into the $1f_{7/2}$ orbital with practically no contribution from the $(0h_{9/2})^3$ configuration; the wave function of the $7/2_2^-$ is dominated by the $(0h_{9/2})^3$ configuration with practically no contribution from the $(0h_{9/2})^2 1f_{7/2}$ configuration. As the strength of $\langle 0h_{9/2}, 0h_{9/2} | \hat{V} | 0h_{9/2}, 1f_{7/2} \rangle_{J=2}$ increases, the two dominant configurations start to interchange between the two states. The increase of the $(0h_{9/2})^3$ configuration in the wave function of the $7/2_1^-$ state allows for the higher $E2$ transition rate to the ground state. This increase also lowers the excitation energy of the state, bringing it closer to the experimental value. On the other hand, the decrease of the $(0h_{9/2})^3$ configuration in $7/2_2^-$ decreases the $E2$ strength to the ground state; however, it has a minimal effect on the excitation energy of this state. The variation of $\langle 0h_{9/2}, 0h_{9/2} | \hat{V} | 0h_{9/2}, 1f_{7/2} \rangle_{J=2}$ introduces mixing between the two original states, but does not influence

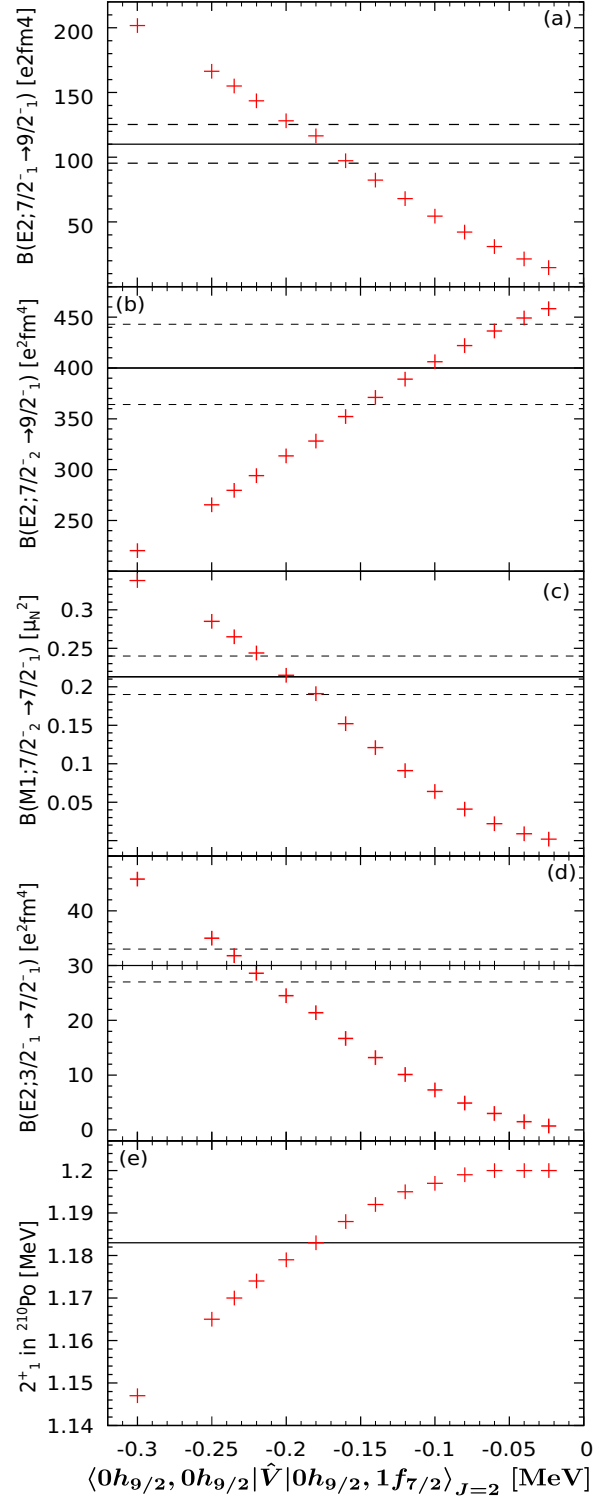


FIG. 6. The dependence of KHP-calculated (a) $B(E2; 7/2_1^- \rightarrow 9/2_1^-)$, (b) $B(E2; 7/2_2^- \rightarrow 9/2_1^-)$, (c) $B(M1; 7/2_2^- \rightarrow 7/2_1^-)$, (d) $B(E2; 3/2_1^- \rightarrow 7/2_1^-)$ in ^{211}At , and (e) the excitation energy of 2_1^+ state in ^{210}Po on the $\langle 0h_{9/2}, 0h_{9/2} | \hat{V} | 0h_{9/2}, 1f_{7/2} \rangle_{J=2}$ TBME. The solid lines represent to experimental values and the dashed lines represent the lower and higher uncertainty limits.

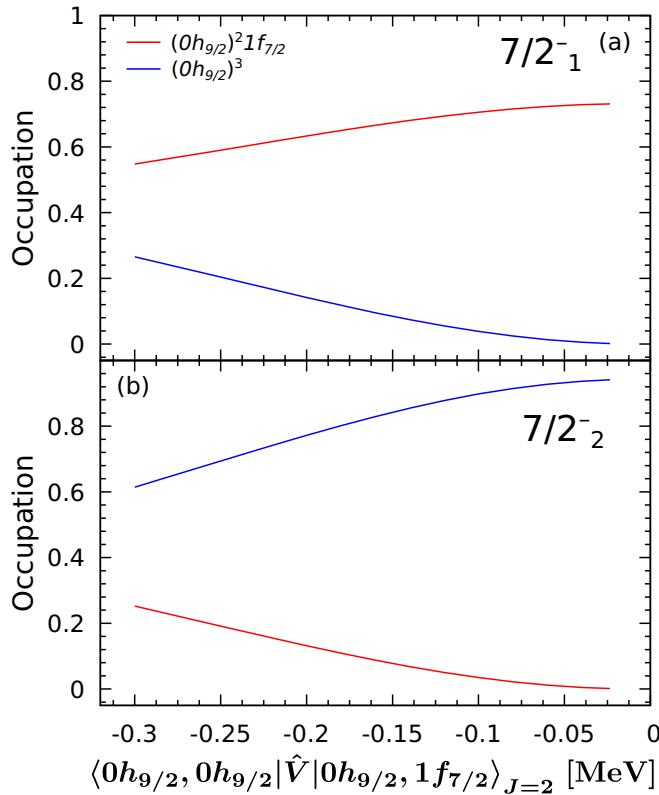


FIG. 7. Occupation number of the main configuration for the (a) $7/2_1^-$ and (b) $7/2_2^-$ states as a function of the $\langle 0h_{9/2}, 0h_{9/2} | \hat{V} | 0h_{9/2}, 1f_{7/2} \rangle_{J=2}$ TBME.

significantly the configurations of other states. It is worth mentioning that a similar mixing between the $7/2_1^-$ and $7/2_2^-$ states can be also achieved if the single-particle energies of the $0h_{9/2}$ and $1f_{7/2}$ orbitals are brought closer together, either by raising the energy of $0h_{9/2}$ and/or lowering the one of $1f_{7/2}$. However this comes at an expense of poorer reproduction of excited state energies.

To conclude, by increasing the strength of $\langle 0h_{9/2}, 0h_{9/2} | \hat{V} | 0h_{9/2}, 1f_{7/2} \rangle_{J=2}$ a much better description of the structure of ^{210}Po and ^{211}At could be achieved. A possible explanation for this could be that this TBME is influenced by some additional excitations not present in the KHP model space. Those excitations have to be $J = 2$ in order to effect this TBME. A more thorough theoretical research needs to be performed in order to understand the origin of the enhanced strength of the $\langle 0h_{9/2}, 0h_{9/2} | \hat{V} | 0h_{9/2}, 1f_{7/2} \rangle_{J=2}$ TBME.

An interesting result comes from the measured lifetime of the $13/2_1^+$ state. If one assumes a pure $M2$ transition, the value of $B(M2; 13/2_1^+ \rightarrow 9/2_1^-) = 38_{-8}^{+7} \mu_N^2 \text{fm}^2$ is obtained. This value is very similar to $B(M2; 13/2_1^+ \rightarrow 9/2_1^-) =$

$38(5) \mu_N^2 \text{fm}^2$ in ^{209}Bi reported in Ref. [42]. With an effective magnetic operator, as derived in the framework of the theory of finite Fermi systems [43,44], a value of $33 \mu_N^2 \text{fm}^2$ is derived for a transition between the $0i_{13/2}$ and $0h_{9/2}$ orbitals in ^{209}Bi . This result coincides with the experimental values for both ^{209}Bi and ^{211}At and shows that the addition of two protons to ^{209}Bi does not affect considerably the $B(M2; 13/2_1^+ \rightarrow 9/2_1^-)$ value, which in both nuclei can be considered as a single-particle transition between the $0i_{13/2}$ and $0h_{9/2}$ proton orbitals.

V. CONCLUSION AND OUTLOOK

Lifetimes of low-energy states in ^{211}At have been measured using the RDDS and DSA methods. The obtained reduced transition probabilities have been compared to two shell-model calculations, one using the Kuo-Herling residual interaction and the other using a single- j approximation for protons in the $0h_{9/2}$ orbital. The KHP calculation, which account only for single particle-hole excitations, significantly overestimates some of the ground-state transition probabilities, especially the $B(E2; 13/2_1^- \rightarrow 9/2_1^-)$ value. This discrepancy has been attributed to the presence of higher-order particle-hole excitations in the wave function of the ground state, which are not accounted for by KHP. The effects of those excitations on the transition rates, however, are weaker in ^{211}At than they are in ^{210}Po . A modification of the $\langle 0h_{9/2}, 0h_{9/2} | \hat{V} | 0h_{9/2}, 1f_{7/2} \rangle_{J=2}$ TBME has been introduced which leads to a considerably better description of the structure of ^{210}Po and ^{211}At . However, the origin of this effect needs to be further investigated. The newly obtained reduced transition probabilities are described very well by a single- j calculation. This, together with the fact that the energy spectrum of ^{211}At is also well described, indicates that seniority can be regarded as a good quantum number in ^{211}At . It would be of interest to continue the same study along heavier $N = 126$ isotones, where information on most $E2$ transitions is still missing.

ACKNOWLEDGMENTS

J.J. and P.V.I. acknowledge the financial support from the Inter-university Attraction Poles Program of the Belgian State-Federal Office for Scientific and Cultural Affairs (IAP Grant No. P7/12) and from GANIL (Caen France) where the origin of this work was laid. G.R. acknowledges the support by Bulgarian Ministry of Education and Science under Grant No. D01-374/18.12.2020. V.K. acknowledge the financial support of NSCRC. Support of the University of Cologne in operating the Tandem accelerator is acknowledged.

- [1] M. G. Mayer, *Phys. Rev.* **78**, 16 (1950).
- [2] G. H. Herling and T. T. S. Kuo, *Nucl. Phys. A* **181**, 113 (1972).
- [3] T. Hamada and I. D. Johnson, *Nucl. Phys.* **34**, 382 (1962).

- [4] S. Bonger, T.T.S. Kuo, and L. Coraggio, *Nucl. Phys. A* **684**, 432 (2001).
- [5] M. Hjorth-Jensen, T. T.S. Kuo, and E. Osnes, *Phys. Rep.* **261**, 125 (1995).

- [6] R. Machleidt, K. Holinde, and Ch. Elster, *Phys. Rep.* **149**, 1 (1987).
- [7] D. R. Entem and R. Machleidt, *Phys. Rev. C* **68**, 041001(R) (2003).
- [8] R. B. Wiringa, V. G. J. Stoks, and R. Schiavilla, *Phys. Rev. C* **51**, 38 (1995).
- [9] J. B. McGrory and T.T.S. Kuo, *Nucl. Phys. A* **247**, 283 (1975).
- [10] T. R. McGoram, G. D. Dracoulis, A. P. Byrne, A. R. Poletti, and S. Bayer, *Nucl. Phys. A* **637**, 469 (1998).
- [11] E. K. Warburton and B. A. Brown, *Phys. Rev. C* **43**, 602 (1991).
- [12] L. Coraggio, A. Covello, A. Gargano, N. Itaco, and T. T. S. Kuo, *Phys. Rev. C* **58**, 3346 (1998).
- [13] E. Caurier, M. Rejmund, and H. Grawe, *Phys. Rev. C* **67**, 054310 (2003).
- [14] H. Naïdja, *Phys. Rev. C* **103**, 054303 (2021).
- [15] D. Kocheva, G. Rainovski, J. Jolie, N. Pietralla, C. Stahl, P. Petkov *et al.*, *Phys. Rev. C* **93**, 011303(R) (2016).
- [16] D. Kocheva, G. Rainovski, J. Jolie, N. Pietralla, A. Blazhev, R. Altenkirch *et al.*, *Phys. Rev. C* **96**, 044305 (2017).
- [17] A. Yaneva *et al.*, *Eur. Phys. J. A* **56**, 246 (2020).
- [18] D. Kalaydjieva, D. Kocheva, G. Rainovski, V. Karayonchev, J. Jolie, N. Pietralla, M. Beckers, A. Blazhev, A. Dewald, M. Djongolov, A. Esmaylzadeh, C. Fransen, K. A. Gladnishki, A. Goldkuhle, C. Henrich, I. Homm, K. E. Ide, P. R. John, R. Kern, J. Kleemann *et al.*, *Phys. Rev. C* **104**, 024311 (2021).
- [19] D. Kocheva *et al.*, *Eur. Phys. J. A* **53**, 175 (2017).
- [20] V. Karayonchev, A. Blazhev, A. Esmaylzadeh, J. Jolie, M. Dannhoff, F. Diel, F. Dunkel, C. Fransen, L. M. Gerhard, R.-B. Gerst, L. Knafla, L. Kornwebel, C. Müller-Gatermann, J.-M. Régis, N. Warr, K. O. Zell, M. Stoyanova, and P. Van Isacker, *Phys. Rev. C* **99**, 024326 (2019).
- [21] A. Dewald, O. Mäller, and P. Petkov, *Prog. Part. Nucl. Phys.* **67**, 786 (2012).
- [22] T. K. Alexander and A. Bell, *Nucl. Instrum. Methods* **81**, 22 (1970).
- [23] B. Singh, D. Abriola, C. Baglin, V. Demetriou, T. Johnson, E. McCutchan, G. Mukherjee, S. Singh, A. Sonzogni, and J. Tuli, *Nucl. Data Sheets* **114**, 661 (2013).
- [24] D. B. Fossan and E. K. Warburton, *Pure Appl. Phys.* **40**, 307 (1974).
- [25] P. J. Nolan and J. F. Sharpey-Schafer, *Rep. Prog. Phys.* **42**, 1 (1979).
- [26] C. Stahl, J. Leske, M. Lettmann, and N. Pietralla, *Comput. Phys. Commun.* **214**, 174 (2017).
- [27] S. Agostinelli *et al.*, *Nucl. Instrum. Methods Phys. Res. A* **506**, 250 (2003).
- [28] J. F. Ziegler, M. D. Ziegler, and J. P. Biersack, *Nucl. Instrum. Methods Phys. Res. A* **268**, 1818 (2010).
- [29] J. Keinonen, in *Capture Gamma-Ray Spectroscopy and Related Topics-1984: 5th International Symposium*, edited by S. Raman, AIP Conf. Proc. No. 125 (AIP, New York, 1985), p. 557.
- [30] A. Winther, *Nucl. Phys. A* **572**, 191 (1994).
- [31] R. Yanez and W. Loveland, *Phys. Rev. C* **91**, 044608 (2015).
- [32] D. Venos, I. Adam, N. A. Bonch-Osmolovskaja, P. Caloun, K. I. Erohina, Y. I. Isakov, O. D. Kjostarova, V. A. Morozov, Ju V. Norseev, and V. I. Stegajlov, *J. Phys. G: Nucl. Part. Phys.* **16**, 1009 (1990).
- [33] S. Bayer, A. P. Byrne, G. D. Dracoulis, A. M. Baxter, T. Kibédi, and F. G. Kondev, *Nucl. Phys. A* **694**, 3 (2001).
- [34] I. Bergström, B. Fant, C. J. Herrlander, P. Thieberger, K. Wikström, and G. Astner, *Phys. Lett. B* **32**, 476 (1970).
- [35] G. Astner, *Phys. Scr.* **5**, 31 (1972).
- [36] M. Shamsuzzoha Basunia, *Nucl. Data Sheets* **121**, 561 (2014).
- [37] O. Häusser, T. K. Alexander, J. R. Beene, E. D. Earle, A. B. McDonald, F. C. Khanna, and I. S. Towner, *Nucl. Phys. A* **273**, 253 (1976).
- [38] I. Talmi, *Simple Models of Complex Nuclei* (Harwood, Chur, 1993).
- [39] M. Stoyanova *et al.*, *Phys. Rev. C* **100**, 064304 (2019).
- [40] B. A. Brown and W.D.M. Rae, *Nucl. Data Sheets* **120**, 115 (2014).
- [41] N. Shimizu, T. Mizusaki, Y. Utsuno, and Y. Tsunoda, *Comput. Phys. Commun.* **244**, 372 (2019).
- [42] O. J. Roberts *et al.*, *Phys. Rev. C* **93**, 014309 (2016).
- [43] P. Ring, R. Bauer, and J. Speth, *Nucl. Phys. A* **206**, 97 (1973).
- [44] R. Bauer, J. Speth, V. Klemm, P. Ring, E. Werner, and T. Yamazaki, *Nucl. Phys. A* **209**, 535 (1973).